AIAA JOURNAL
Vol. 40, No. 9, September 2002

Numerical Study of Blast-Wave Propagation in a Double-Bent Duct

S. M. Liang* and K. C. Weng†
National Cheng Kung University, Tainan 701, Taiwan, Republic of China
and
K. Takayama‡
Tohoku University, Sendai 980-8577, Japan

A high-resolution Euler solver has been used to investigate the flowfield induced by a blast wave in a double-bent duct. A blast-wave/vortex interaction and shock/shock interactions are also studied. A pair of vortices with an opposite rotating direction is found. The trajectories of the induced main vortices are explored for different initial pressure ratios. It was found that the vortex could deform the shock front of the blast wave because of compression and expansion involved in their interaction. Moreover, after blast-wave diffraction around the first convex corner a locally maximum wall pressure could occur at the second concave corner, and a globally maximum wall pressure could occur at the first concave corner, resulting in a large loading at the compression corners.

Introduction

ENGINEERS and scientists are quite interested in the problem of blast-wave propagation in ducts because the phenomena of blast-wave propagation often take place, for example, in the exhaust pipes of internal combustion engines or, caused by explosions, inside a building. A fundamental study of blast-wave propagation in a duct is helpful in the understanding of the blast-wave dynamics. In this study we investigated the unsteady flow of planar blast-wave propagation in a double-bent duct with two 90-deg turns. The problem involved a complicated unsteady flowfield of blast-wave/vortex interactions, shock/shock interactions, and blast-wave reflections.

In the past there were very few papers that reported the detail of the flowfield induced by a blast wave in a double-bent duct. Some related papers are referred to here. Howard and Mathews[1] experimentally investigated the vortex generation caused by shock-wave diffraction around a corner. Schardin[2] studied a reflected shock/vortex interaction by using the shadowgraph method. His experimental results provided basic understanding of shock/vortex interaction. Mandella et al.[3] conducted a series of experiments for studying the vortex induced by a shock wave near a corner. They reported that the vortex generation was not caused by the fluid viscosity. Sivier et al.[4] numerically simulated the problem studied by Schardin and obtained good agreement between the numerical and experimental results. Igra et al.[5] used both experimental and numerical methods to study the intensity of a diffracted wave in a branched duct and concluded that the flow behind the diffracted wave could not be assumed to be quasi-one-dimensional. Ellzey and Henneke[6] investigated the sound generation caused by the shock/vortex interaction and its mechanism. They found that the shock-wave deformation and a compression effect involved in the interaction are the two main factors for sound generation. Grasso and Pirozzoli[7] numerically studied a shock/vortex interaction and classified the interaction into three types. They also characterized the shock and vortex deformations and the mechanism of sound generation in the interaction of a cylindrical shock wave with a vortex. The numerical scheme they used is a weighted essentially nonoscillatory (WENO) scheme of Jiang and Shu.[8] Inoue and Hattori[9] studied a shock/vortex interaction by a sixth-order compact Pade scheme for spatial discretization. They reported the detailed mechanism of the flowfield at an early stage of the interaction. Ofengeim and Drikakis[10] used an adaptive-grid method and a second-order Godunov scheme to simulate planar blast-wave propagation over a cylinder. Their result revealed that the blast-wave duration significantly influences the unsteady flow over the cylinder. Grönig[11] reported shock/vortex interactions with some holographic and color schlieren pictures. These pictures could provide us some understanding of the shock/vortex interaction. There were other papers in the proceedings of the second international workshop on shock wave/vortex interaction. Because of the space limitation, those papers are omitted here. Yang[12] observed the flowfield of shock-wave propagation in a double-bent duct by using the holographic interferometry. All references just mentioned are related with shock-wave/vortex interactions.

Because a blast wave has the jump characteristics of a shock wave associated with expansion waves behind it, a WENO scheme of Jiang and Shu[8] is employed in this study. The WENO scheme possesses a high-resolution ability of capturing discontinuities. The working fluid is assumed to be air. The duct geometry is schematically shown in Fig. 1. Two distance parameters s_1 and s_2 are chosen. The parameter s_1 is used to measure the distance from the first convex corner along the lower wall. The parameter s_2 is the distance from the first concave corner along the upper wall. Thus $s_1 = 0$ denotes the first convex corner, $s_1 = 1$ the second concave corner, $s_2 = 0$ the first concave corner, and $s_2 = 1$ the second convex corner. At the duct outlet $s_1 = 2.5$ denotes the lower-wall exit and $s_2 = 2$ for the upper-wall exit.

Mathematical Formulation and Numerical Method

Based on the experimental data of Yang,[12] the vortices generated in the diffraction problem of weak shocks around a sharp convex corner are relatively small compared with the main vortex caused by the shock diffraction. Thus we neglect the effects of external forces and the fluid viscosity. The neglect of the viscous effect can save a lot of computational time and computer memory. Consequently the equations governing the blast-wave propagation in the duct are the continuity, momentum, and energy equations. Thus, the Euler equations are used in this study.

The numerical method of the high-order scheme of Jiang and Shu[8] in a finite volume approach with an extension to curvilinear coordinates is used for solving the Euler equations. Namely, a fourth-order Runge–Kutta method is used for time integration, and a WENO-LF-5 scheme is used for spatial discretization, where LF denotes the global Lax–Friedrichs flux splitting and 5 denotes fifth-order accuracy. A global time step is chosen for unsteady flow

Received 26 April 2001; revision received 2 April 2002; accepted for publication 22 April 2002.

*Professor, Institute of Aeronautics and Astronautics. Associate Fellow AIAA.
†Graduate Student, Institute of Aeronautics and Astronautics.
‡Professor, Shock Wave Research Center, Institute of Fluid Science.

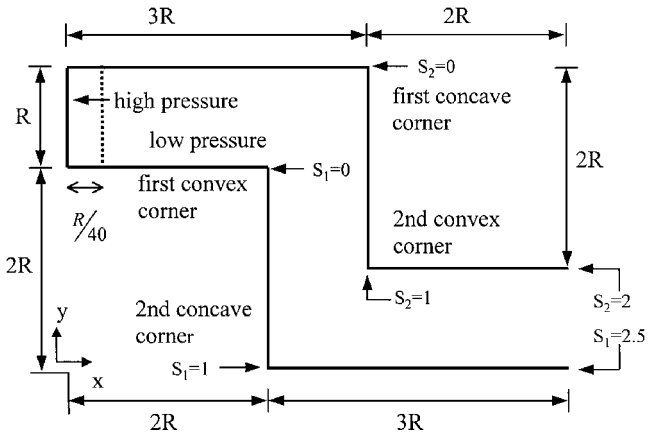

Fig. 1 Schematic diagram of a double-bent duct.

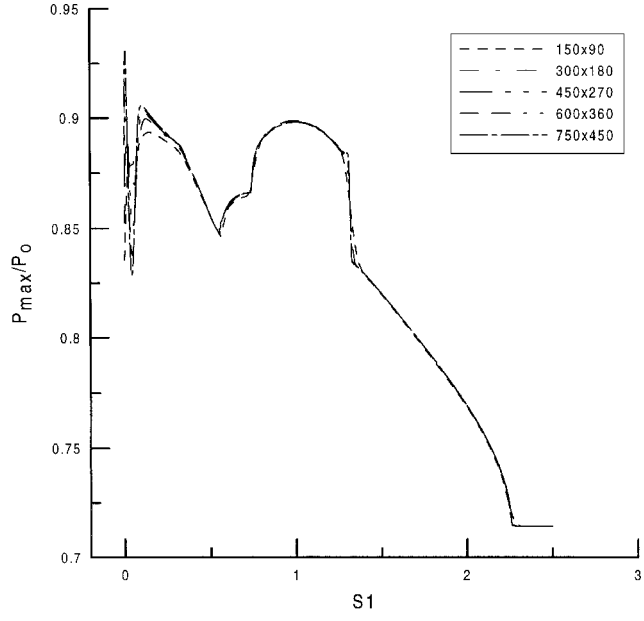

Fig. 2 Effect of grid number on the recorded maximum wall pressures on the lower wall.

calculations. Namely, a minimum time step of local time steps over the computational domain is used for unsteady flow calculations. Initially, the rupture of a high-pressure region produced a blast wave, which would propagate downstream into a quiet air. The boundary condition imposed on the duct wall is the tangency condition. Three ghost points are used outside the wall. The flow properties at these ghost points are symmetric with respect to the wall. At the duct exit the flow condition is specified by the initial flow condition because all computations will be terminated before the blast wave passes through the duct exit. At $x = 0$ it is a closed end.

Results and Discussion

Code Validation

The present computer code has been quantitatively validated on several test problems such as shock-wave reflection from a wedge.[13] Moreover, the problem shock-wave diffraction around a 90-deg corner was calculated to verify the ability of capturing the downstream wall shock because there existed the experimental data of the downstream wall shock wave.[14] The incident shock Mach numbers at the corner are 1.5 and 2; our computed wall shock Mach numbers are 1.12 and 1.26, which agree well with the experimental values of 1.15 and 1.3 (Ref. 14). In addition, for the problem of shock-wave propagation through the double-bend duct, the computed result is compared with the holographic interferograms that were obtained by Yang et al.[15] at the Shock Wave Research Center of Tohoku University. The initial condition of the high pressure p_h and the low pressure p_l is, respectively, given by $p_h = 1.23$ kg/cm^2

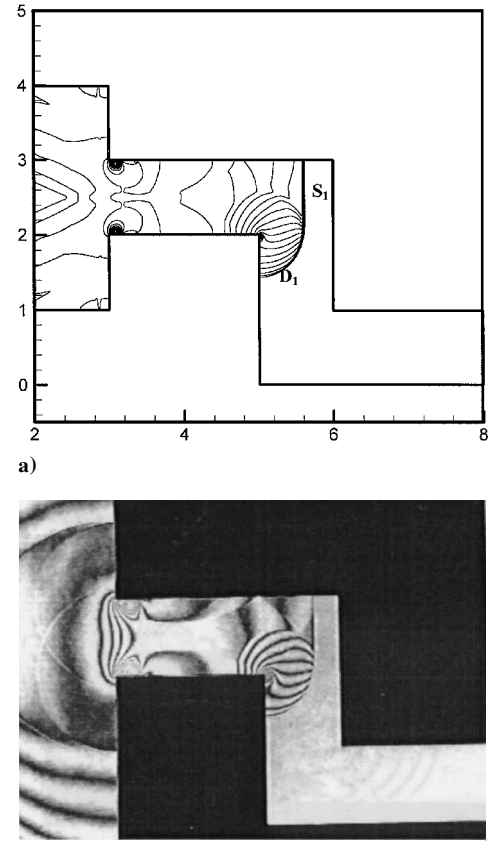

Fig. 3 Comparison of a) computed isopycnics with b) holographic interferograms[15]; $M_s = 1.08$ and $t = 1.85$.

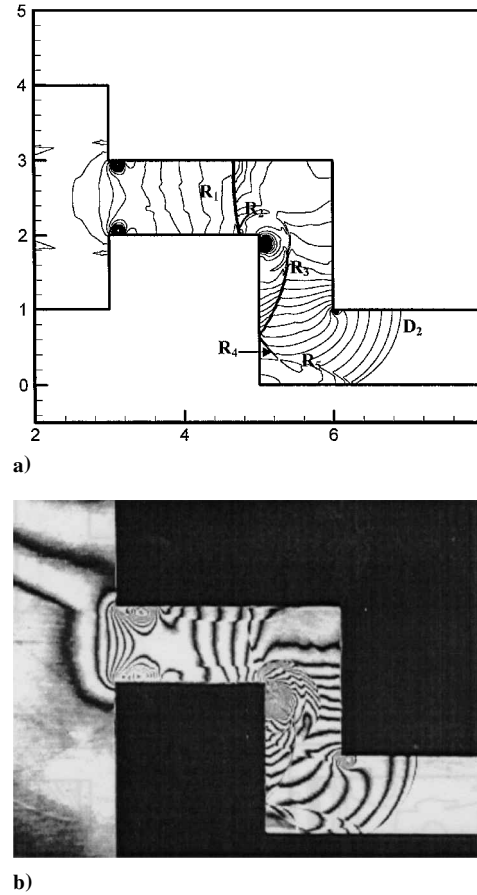

Fig. 4 Comparison of a) computed isopycnics with b) holographic interferograms[15]; $M_s = 1.08$ and $t = 3.70$.

and $p_l = 1$ atm. The pressure ratio produces an incident shock with Mach number of $M_s = 1.08$. The Courant–Friedrichs–Lewy number (CFL) was chosen to be CFL = 0.5. Five grids, 150×90 (grid 1), 300×180 (grid 2), 450×270 (grid 3), 600×360 (grid 4), and 750×450 (grid 5), were chosen for studying the grid effect on the numerical solution. We checked the changes of the recorded maximum wall (dimensionless) pressures on the lower wall by subsequent grid refinement from grid 1. It was found that the largest peak and lowest valley occurred at $s_1 = 0.05$ and 0.11, respectively, as shown in Fig. 2. The changes of the peak value caused by subsequent grid refinement is 0.62% for grid 2, 0.52% for grid 3, 0.17% for grid 4, and 0.087% for grid 5. The change in the lowest valley as a result of subsequent gird refinement is −9.4% for grid 2, −2.3% for grid 3, −1.3% for grid 4, and −0.6% for grid 5. Because the changes in the largest peak and lowest valley are very small on grid 4, grid 4 is used for the test problem and for the subsequent study. For the test problem it was found that the computed maximum wall pressure at the second concave corner ($s_1 = 1$) is 0.898 for the five grids.

Figures 3 and 4 show the comparison of the computed isopycnics with the holographic pictures at the dimensionless times $t = 1.85$ and 3.70, respectively. The dimensionless times t correspond to the dimensional time of $t = 100$ and 200 μs in experiments. At $t = 1.85$ the incident shock wave has passed through the first convex corner ($s_1 = 0$). This convex corner causes the incident shock wave S_1 to diffract, resulting in the expansion waves emitting from the corner and the diffracted shock wave D_1, as shown in Fig. 3. At $t = 3.70$ the second convex corner ($s_2 = 1$) induces another diffracted shock

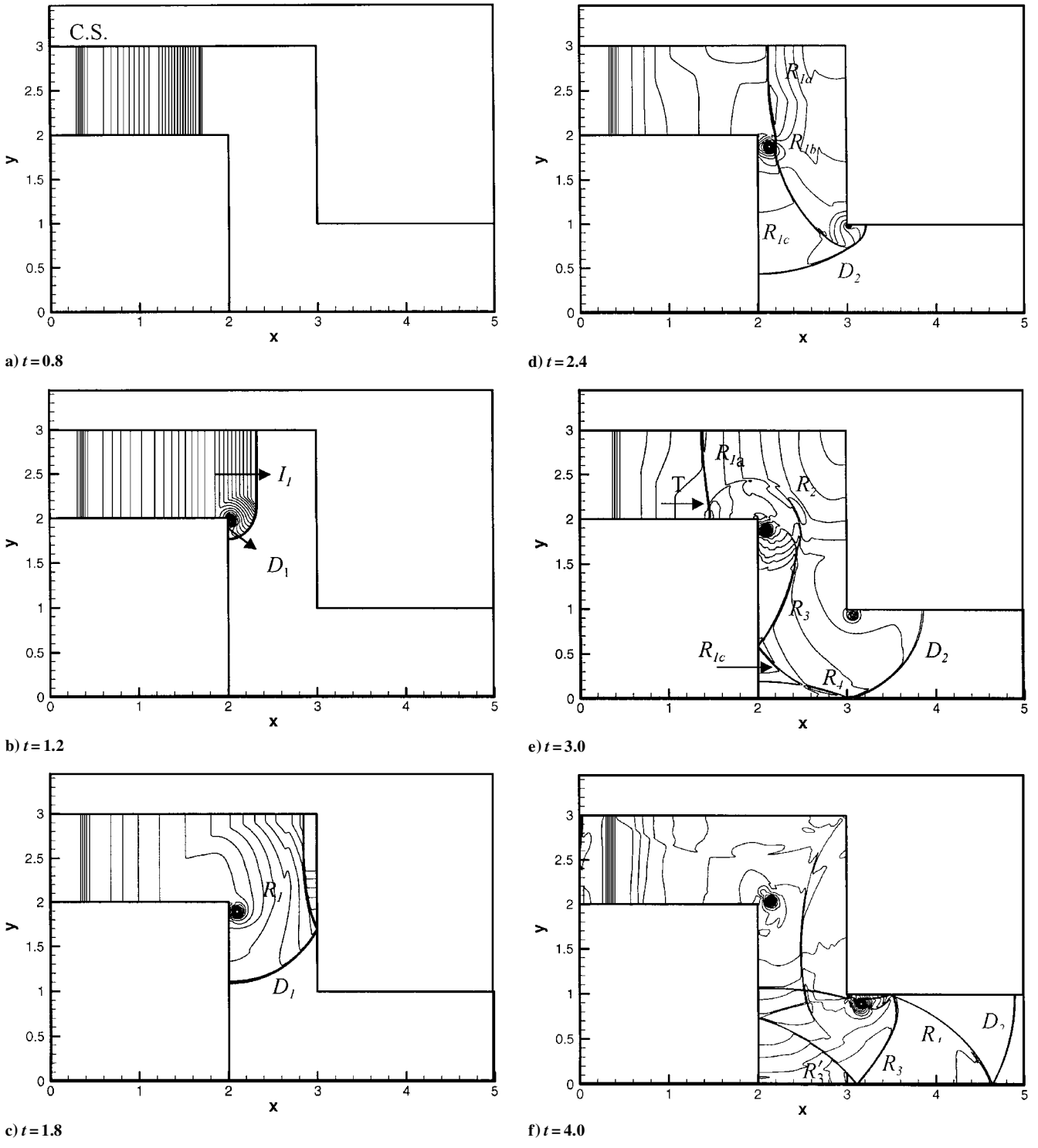

a) $t = 0.8$ **d)** $t = 2.4$

b) $t = 1.2$ **e)** $t = 3.0$

c) $t = 1.8$ **f)** $t = 4.0$

Fig. 5 Flow patterns of iospycnic at different instants, $p_h/p_l = 40$.

wave D_2 and its reflected wave R_5, as shown in Fig. 4. The reflected shock wave R_1 of the incident shock S_1 has entered the upstream duct, resulting in a single Mach reflection with the rereflected shock wave R_2. On the other hand, a part of the reflected shock wave is reflected again from the left wall to become the rereflected shock waves R_3 and R_4 that intersect at the reflection point on the left wall.

Blast-Wave Propagation in the Double-Bent Duct

To generate a planar blast wave, we consider a high-pressure region, located near $x = 0$, as shown in Fig. 1. The region has a width of $R/40$, where R is the duct width. A blast wave is generated by rupture of a diaphragm that separates the high-pressure and the low-pressure regions. The temperatures in the both regions were chosen to be the same. The blast wave will propagate into the downstream duct. The initial pressure ratio p_h/p_l is assumed to be 40, which can generate a blast wave with intensity of shock Mach number of $M_s = 1.55$ right before the first convex corner.

Flowfields of Density and Pressure

Figure 5 shows the flow patters of isopycnics at different (dimensionless) instants. At $t = 0.8$ the blast wave has arrived at $x = 1.7$, as shown in Fig. 5a, and a series of expansion waves followed the shock front. A contact surface is developed near $x = 0.35$, which was verified by checking the pressure and density distributions across the contact surface. On the contact surface the pressure is continuous, but not the density. At $t = 1$ the blast wave has moved to the first convex corner and will start to diffract. At $t = 1.2$, as shown in Fig. 5b, the blast wave consists of two parts. One is the straight part I_1, the incident wave. The other is the curved diffracted part D_1. Because of the wave diffraction, a vortex is formed near the corner. The mechanism of vortex generation will be discussed later. Moreover, the convex corner also produces circular expansion waves behind the incident blast wave. The leading expansion wave, the diffracted wave, and the incident blast wave intersect together. At $t = 1.8$ the incident blast wave is reflected from the right wall. The reflected blast wave is denoted by R_1, as shown in Fig. 5c. The diffracted wave D_1 is propagating downstream. At $t = 2.2$ the diffracted wave arrives at the second convex corner and will start a second diffraction there. At $t = 2.4$ the reflected blast wave starts to intersect with the vortex, which causes the blast wave to deform, as shown in Fig. 5d. We will discuss the blast-wave/vortex interaction later. At this instant the diffracted wave has passed through the second convex corner and induces a downstream vortex. We also can see the expansion waves near the second convex corner, as occurred at the first convex corner. The reflected blast wave is denoted by three parts, R_{1a}, R_{1b}, and R_{1c}, where R_{1b} is the part that interacts with the vortex. The R_{1c} part intersects the diffracted wave D_2 that has diffracted around the second convex corner.

At $t = 2.6$ the reflected blast wave has finished the interaction with the vortex and is entering the upstream duct. At $t = 3$ the reflected blast wave R_{1a} is reflected from the lower wall, forming a single Mach reflection with the triple point T and the rereflected wave R_2, as shown in Fig. 5e. The rereflected wave R_2 is connected with the wave R_3, which is the rereflected wave of the reflected waves R_{1b} and R_{1c}. The diffracted wave is reflected from the lower wall, denoted by R_4. The wave R_4 intersects with the wave R_{1c}. At later times more complicated waves will be developed. At $t = 4$ the wave pattern is shown in Fig. 5f. We can see that the diffracted wave D_2 has moved to the duct exit. The vortices induced by the convex corners are clearly seen. The reflected wave of the diffracted wave D_2 is denoted by the wave R_4. Other reflected waves have encountered twice or triple reflections. The evolution of these waves is complicated and omitted to report here. From Figs. 5a–5f we found that the contact surface always occurred at approximately $x = 0.4$.

The patterns of pressure distributions at different instants corresponding to Fig. 5 are very similar to the density contours in Fig. 5, except for the contact surface. We omit to report them here because of space limitations.

Wall-Pressure Distribution

Because the blast-wave propagation is unsteady and nonlinear, the flow properties, in particular the wall pressures, are changing with time. A maximum wall pressure means that the largest wall pressure over $t \leq 4$ is recorded at a fixed point. We only recorded the maximum wall pressures at every grid point on the upper and lower walls after the first 90-deg turn. Figures 6a and 6b show the recorded maximum wall pressures on the lower s_1 and upper s_2 walls for different initial pressure ratios, respectively. We chose the initial pressure ratio to be $p_h/p_l = 20$, 40, and 60. These ratios produced a shock Mach number of 1.45 for $p_h/p_l = 20$, 1.55 for $p_h/p_l = 40$, and 1.75 for $p_h/p_l = 60$ right before the blast-wave diffraction around the first convex corner. Obviously, a larger value of p_h/p_l produces a stronger blast wave. We use the case of $p_h/p_l = 40$ to describe the variation of the maximum wall pressures because other cases produced a similar result. From Fig. 6a we can see that there is a peak with value of $p_{\max}/p_0 = 2.41$ occurring in the vicinity of the first convex corner, where p_0 denotes the undisturbed pressure. Away from the corner the maximum wall pressure is decreased to 1.20, which occurs at $s_1 = 0.057$. For $s_1 > 0.13$ the maximum wall pressure monotonically decreases from 1.70 to 1.29

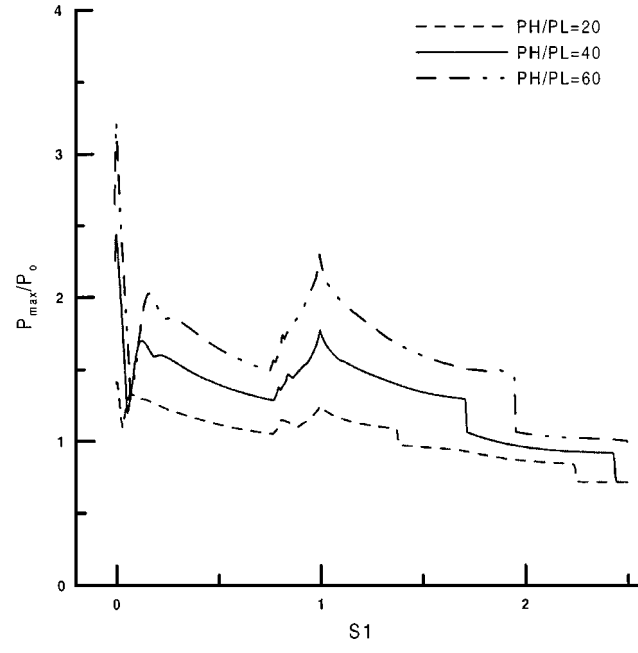

a) Lower wall

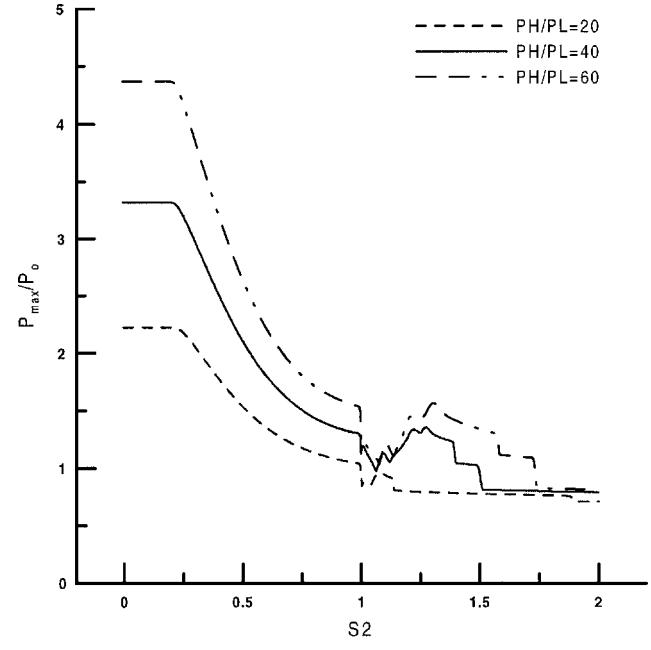

b) Upper wall

Fig. 6 Recorded maximum wall pressures over $t \leq 4$.

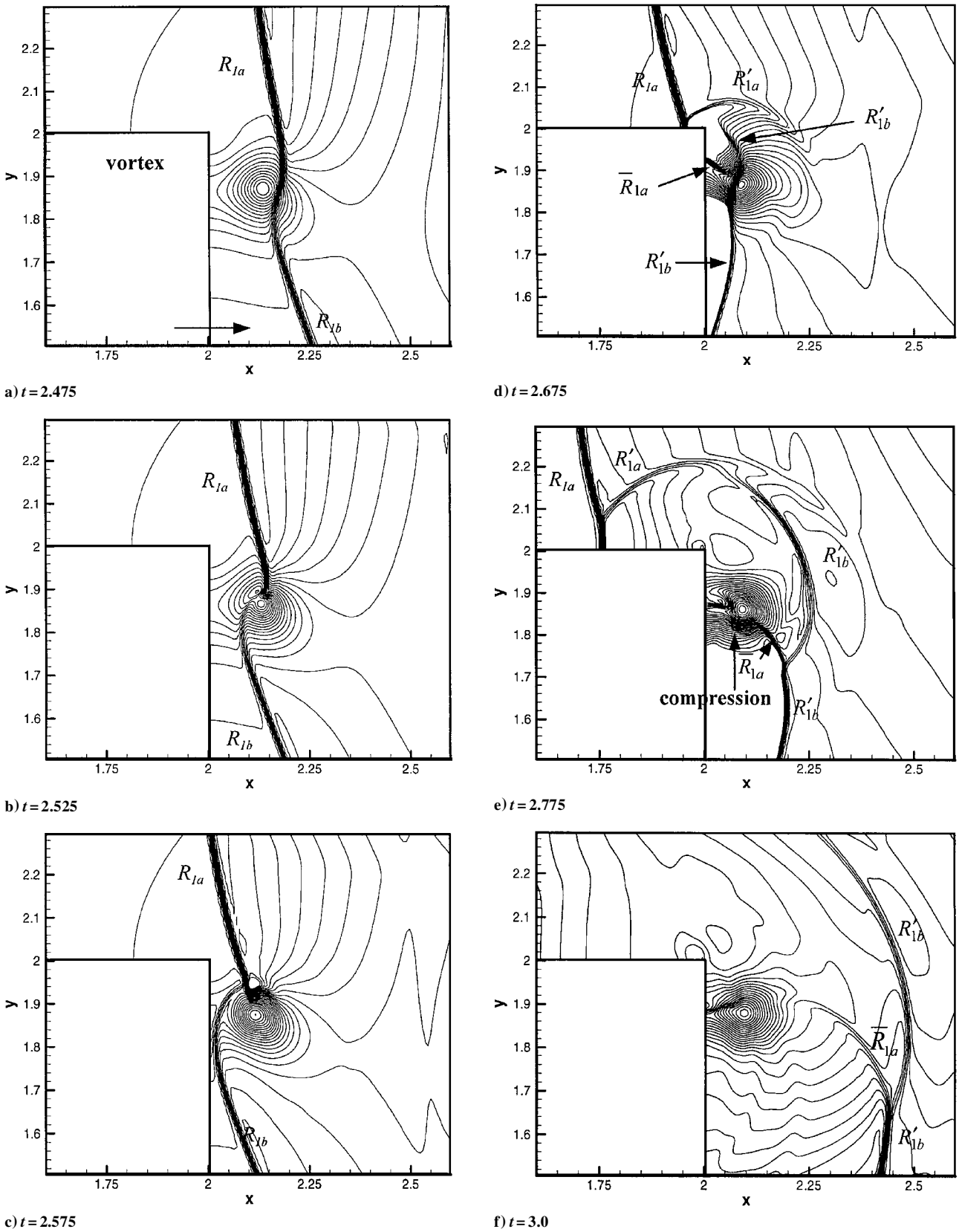

a) $t = 2.475$ d) $t = 2.675$

b) $t = 2.525$ e) $t = 2.775$

c) $t = 2.575$ f) $t = 3.0$

Fig. 7 Pressure contours near the first convex corner when the blast-wave interacted with the induced vortex for $p_h/p_l = 40$.

at $s_1 = 0.77$. For $s_1 > 0.77$ the maximum wall pressure starts to increase to the second peak with $p_{max}/p_0 = 1.77$ at $s_1 = 1$, the second concave corner. For $s_1 > 1$ the maximum wall pressure with two jumps is monotonically decreased to the initial pressure at downstream. The pressure jump was caused by a reflection of blast wave.

Along the upper wall the maximum wall pressure is constant for $0 < s_2 < 0.25$ and then decreases to the lowest value of 0.98 at $s_2 = 1.06$, where it is almost the second convex corner. After that, the maximum wall pressure increases to a peak value of 1.35 at $s_2 = 1.26$ and then decreases to the initial pressure at downstream.

In summary, the maximum wall pressure in the vicinity of the two convex corners is the lowest value of maximum wall pressures, and the maximum wall pressure at the second concave corner is locally a peak value, compared with those at the neighboring regions.

Blast-Wave/Vortex Interaction

Vorticity Generation

The vorticity production in the double-bent duct is mainly caused by the blast-wave diffraction. Other vorticity productions generated by the nonuniformity of entropy induced by curved shock waves are relatively small, compared with that for the main vortex induced by the blast-wave diffraction. The reason is that the entropy increase behind curved shock waves is of third order for weak shock waves. We can use a vorticity transport equation to explain the vorticity generation along a particle path. For an inviscid, two-dimensional flow with shock waves, we can easily derive the following vorticity transport equation:

$$\frac{\mathrm{D}\omega}{\mathrm{D}t} = -\omega(\nabla \cdot \boldsymbol{V}) - \frac{\nabla p \times \nabla \rho}{\rho^2}$$

where ω denotes the vorticity and $\omega = \nabla \times \boldsymbol{V}$ and ∇ the gradient operator. The mechanism of vorticity production is attributed to two parts. One is caused by the flow compressibility, the divergence of $\boldsymbol{V}$ $(\nabla \cdot \boldsymbol{V})$, that is, the fluid dilatation. The other is caused by the baroclinic effect, $\nabla p \times \nabla \rho$. During the blast-wave diffraction, the flow near the corner is in expansion, and the wave front is being elongated, resulting in a curved nonuniform wave front. Consequently the flow behind the curved wave front has the pressure and density gradients and generates a nonzero value of $\nabla p \times \nabla \rho$.

Blast-Wave Deformation

When the reflected blast wave interacts with the vortex caused by the first convex corner, the blast wave encounters two different processes of interaction, resulting in blast-wave deformation. Figure 7 shows the process of the reflected blast wave interacting with the vortex. The detail of the vortex induced by the blast wave is described next.

Figure 7a shows that the blast wave enters the vortex region and starts to deform. The wave deformation involves two processes: compression and expansion. The upper part of the blast wave in the vortex region encounters a compression (deceleration) effect because the vortex flow direction is in a clockwise direction, which is opposite to the direction of the moving blast wave. The lower part of the blast wave in the vortex region encounters an expansion (acceleration) effect because the flow direction is the same as the direction of the moving blast wave, as shown in Fig. 7b. Because the lower part of the blast wave in the vortex region moves faster than the upper part, the lower part will move faster away from the vortex core than the upper part. Figure 7c shows the flowfield at $t = 2.575$. We can see that the lower part of the blast wave has already moved away from the vortex core, but the upper part still interacts with the vortex core. At $t = 2.675$ the upper part of the reflected blast wave R_{1a} has entered the horizontal duct, resulting in a single Mach reflection, as shown in Fig. 7d. The reflected part of the wave R_{1a} is denoted by the wave R'_{1a}. A partial wave $\bar{R}_{1a}$ of the wave R_{1a} intercepted by the corner remains in the vortex region. This remaining wave $\bar{R}_{1a}$ is interacting with the reflected wave R'_{1b} of the blast wave R_{1b}. The waves R'_{1a} and R'_{1b} are disconnected. At later time, $t = 2.775$, the two waves R'_{1a} and R'_{1b} are connected together, as shown in Fig. 7e. The remaining wave $\bar{R}_{1a}$ penetrates the vortex core and is connected with the wave R'_{1b}, producing a compression region denoted by the black region. At $t = 3$ the blast wave R'_{1b} is away from the vortex region except for the remaining wave $\bar{R}_{1a}$ that is still interacting with the vortex, as shown in Fig. 7f.

Effect of Blast-Wave Intensity on the Induced Vortex

Figure 8 shows the velocity field and the vorticity contour near the first convex corner for different initial pressure ratios. Figure 8a is the case of $p_h/p_l = 20$, Fig. 8b for $p_h/p_l = 40$, and Fig. 8c for $p_h/p_l = 60$. From Fig. 8 one can see that there are two vortices generated with an opposite rotation direction. The upstream vortex has a counterclockwise rotating direction, and the downstream vortex has a clockwise rotating direction. The downstream vortex intensity is stronger than the upstream one. Moreover, the more intense the blast wave, the farther downstream and the stronger the vortex. We call the stronger vortex as a major vortex, and the weaker vortex as a minor vortex.

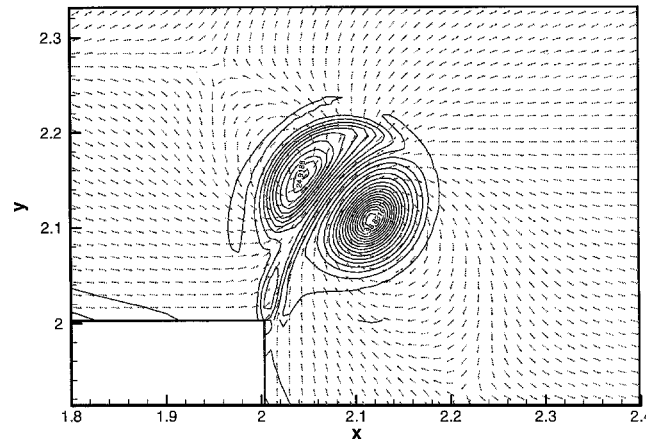

a) $p_h/p_l = 20$

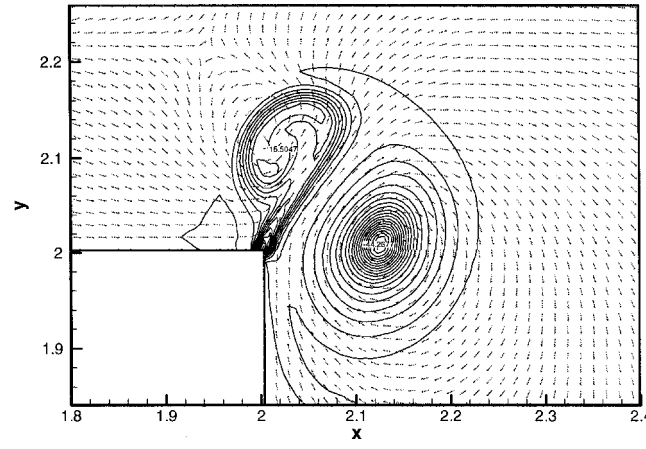

b) $p_h/p_l = 40$

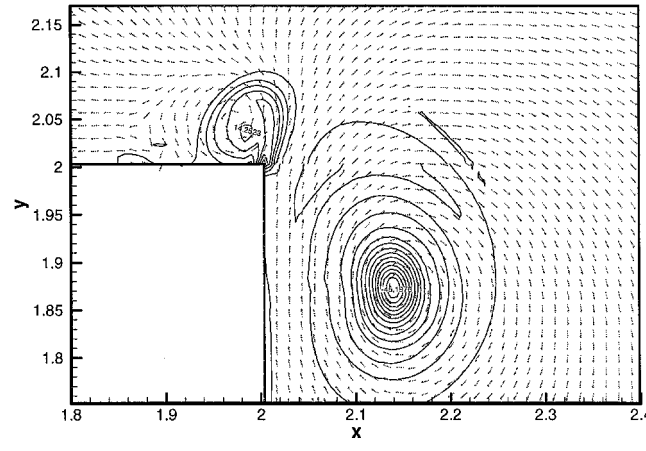

c) $p_h/p_l = 60$

Fig. 8 Vorticity contours and the velocity fields near the first convex corner for different blast-wave intensities at $t = 3.4$.

Vortex Trajectory

The vortex trajectory is described by tracing the major vortex centers at the different instants. Figure 9 shows the vortex trajectories of the downstream vortices near the first and second convex corners, respectively, for different blast-wave intensities. In Fig. 9a the trajectory was recorded from $t = 2$ to 4 with a time increment of $\Delta t = 0.2$. We can see that the vortex center is moved to the right at very early times and then moved toward the left wall for a short while. At later times the vortex center is moved away from the wall. We chose the case of $p_h/p_l = 40$ as an example. The vortex center is moved to the right from $t = 2$ to 2.6 and then moved toward the right wall from $t = 2.4$ to 2.6. For $t > 2.8$ the vortex center is moved away from the wall again. From Fig. 9b we can see the trajectories of the

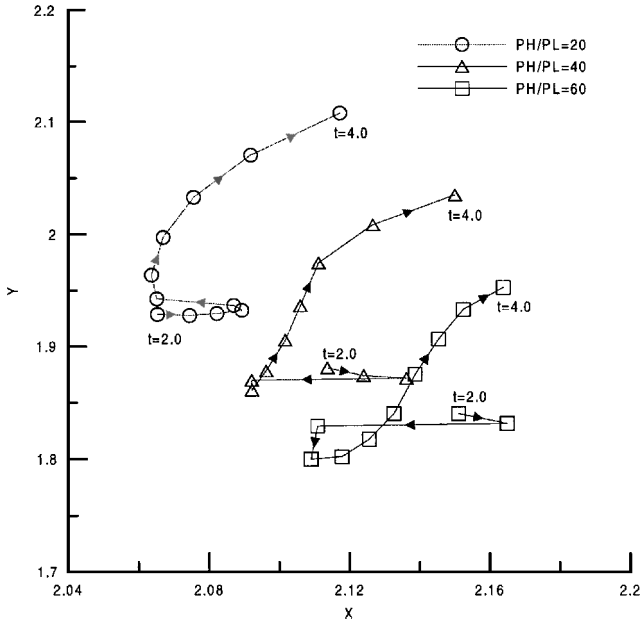

a)

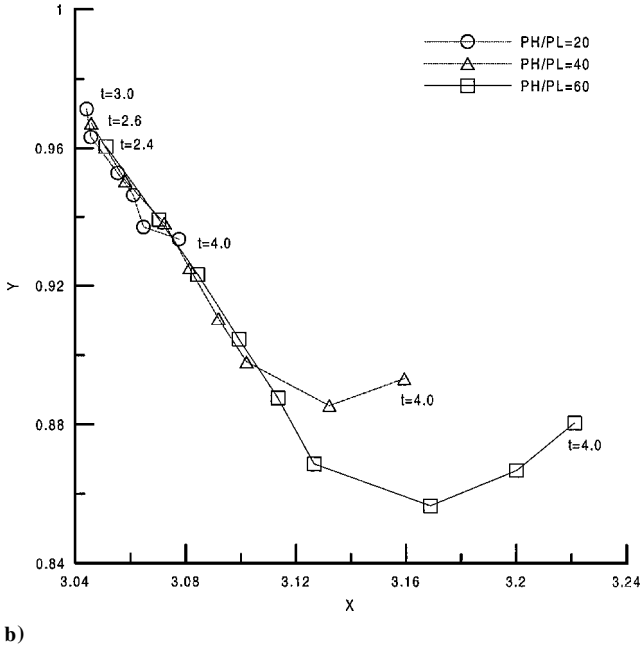

b)

Fig. 9 Trajectories of the vortex centers near the a) first and b) second convex corners for different blast-wave intensities.

vortex centers before $x = 3.10$ are very close for three cases. The vortex centers are located near the upper wall of the downstream horizontal duct, and the plotting time is from $t = 3$ for the case of $p_h/p_l = 20$, $t = 2.6$ for $p_h/p_l = 40$, and $t = 2.4$ for $p_h/p_l = 60$. For these three cases the vortex centers are basically moved downstream with the flow and away from the upper wall. For the cases of $p_h/p_l = 40$ and 60, the vortex centers are turned slightly upward at later times.

Conclusions

A reasonably accurate Euler solver was used to investigate the flowfields induced by blast waves in a double-bent duct. Blast-wave/vortex interactions were studied. The formation and trajectory of the induced vortex were investigated and reported. A pair of vortices with an opposite rotating direction is found. For a stronger blast wave the two vortices consist of one stronger vortex and one weaker vortex. The stronger vortex is located farther downstream than the weaker one. It was found that the vortex could deform the blast wave because of compression involved in their interaction. Moreover, after blast-wave diffraction around the first convex corner there is a locally maximum pressure at the first compression (concave) corner and a globally maximum pressure at the second compression (concave) corner. Namely, the duct wall has larger loading near the compression corners than the neighboring regions.

Acknowledgments

The support for this work under a contract of the National Science Council, NSC 89-2612-E-006-018, is gratefully acknowledged. The authors appreciate A. Abe for his provision of holographic interferograms. The authors are also indebted to the reviewers because of their valuable comments.

References

[1]Howard, L., and Mathews, D., "On the Vortices Produced in Shock Diffraction," *Journal of Applied Physics*, Vol. 27, No. 3, 1956, pp. 223–231.

[2]Oertel, H., *Stossrohre: Theorie, Praxis, Anwendungen, mit einer Einführung in die Physik der Gase*, *Shock Tubes*, Springer-Verlag, New York, 1966, pp. 716–718.

[3]Mandella, M., Moon, Y. J., and Bershader, D., "Quantitative Study of Shock Generated Compressible Vortex Flows," *Proceedings of the 15th International Symposium Shock Waves and Shock Tubes*, edited by D. Bershader and R. Hanson, Stanford Univ. Press, Stanford, CA, 1986, pp. 471–477.

[4]Sivier, S., Loth, E., Baum, J., and Lohner, R., "Vorticity Produced by Shock Wave Diffraction," *Shock Waves*, Vol. 2, No. 1, 1992, pp. 31–41.

[5]Igra, O., Wang, L., Falcovitz, J., and Heilig, W., "Shock Wave Propagation in a Branched Duct," *Shock Waves*, Vol. 8, No. 6, 1998, pp. 375–381.

[6]Ellzey, J. L., and Henneke, M. R., "The Shock-Vortex Interaction: The Origins of the Acoustic Wave," *Fluid Dynamics Research*, Vol. 21, No. 3, 1997, pp. 171–184.

[7]Grasso, F., and Pirozzoli, S., "Shock-Wave-Vortex Interactions: Shock and Vortex Deformations, and Sound Production," *Theoretical Computational Fluid Dynamics*, Vol. 13, No. 6, 2000, pp. 421–456.

[8]Jiang, G. S., and Shu, C. W., "Efficient Implementation of Weighted ENO Schemes," *Journal of Computational Physics*, Vol. 126, No. 1, 1996, pp. 202–228.

[9]Inoue, O., and Hattori, Y., "Sound Generation by Shock-Vortex Interaction," *Journal of Fluid Mechanics*, Vol. 380, Feb. 1999, pp. 81–116.

[10]Ofengeim, D. Kh., and Drikakis, D., "Simulation of Blast Wave Propagation over a Cylinder," *Shock Waves*, Vol. 7, No. 6, 1997, pp. 305–317.

[11]Grönig, H., "Shock Wave/Vortex Interaction," *Proceedings of the 2nd International Workshop on Shock Wave/Vortex Interaction*, edited by K. Takayama and Z. Jiang, Tohoku Univ., Sendai, Japan, 1998, pp. 1–4.

[12]Yang, J., "An Experimental and Theoretical Investigation on the Behavior of Weak Shock Waves," Ph.D. Dissertation, Inst. of Fluid Science, Tohoku Univ., Sendai, Japan, April 1995 (in Japanese).

[13]Liang, S.-M., Hsu, J.-L., and Wang, J.-S., "Numerical Study of Cylindrical Blast-Wave Propagation and Reflection," *AIAA Journal*, Vol. 39, No. 6, 2001, pp. 1152–1158.

[14]Abate, G., and Shyy, W., "Dynamic Structure of Confined Shock Undergoing Sudden Expansion," *Progress in Aerospace Science*, Vol. 38, No. 1, 2002, pp. 23–42.

[15]Yang, J., Onodera, O., and Takayama, K., "Holographic Interferometric Investigation of Shock Wave Diffraction," *Vizualization Society of Japan*, Vol. 14, Suppl. No. 1, July 1994, pp. 85–88.

M. Sichel
Associate Editor